Available online at www.sciencedirect.com
SCIENCE DIRECT®
Building and Environment 41 (2006) 590–601
BUILDING AND ENVIRONMENT
www.elsevier.com/locate/buildenv

The influence of heat capacity and its spatial distribution on the transient wall thermal behavior under the effect of harmonically time-varying driving forces

P.T. Tsilingiris

Department of Energy Engineering, Technological Education Institution (TEI) of Athens, A.Spyridonos str. GR 122 10, Egaleo, Athens, Greece

Received 10 January 2005; received in revised form 11 February 2005; accepted 28 February 2005

Abstract

An analysis was developed for the theoretical investigation of heat capacity and of the effects of its spatial distribution on the thermal behavior of structural walls of uniform thermal resistance. The numerical solution of the governing differential equations under the appropriate initial and boundary conditions, allows the prediction of the time-varying heat flux during the transient heating of walls until quasi steady-state conditions are developed asymptotically. It is derived that as far as the fundamental physical behavior of a clear wall section is concerned, although the time depended heat flux is effectively damped and phased out as the wall heat capacity increases, the average quasi steady-state heat flux is constant, irrespectively of wall heat capacity, incident solar radiation intensity, radiation absorption at the exterior wall surface and particular weather conditions defining wall heat loss or gain. However, even though the average quasi steady-state heat flux is constant irrespectively of the wall heat capacity, its time depended value during the development of transient is strongly influenced by the spatial distribution of heat capacity at a direction perpendicular to the wall plane, something which is determined by the wall time constant.

Keywords: Wall heat capacity; Heat capacity distribution; Thermal time constant; Wall heat transfer

1. Introduction

The effect of building envelope design is vital for the thermal behavior of structures. It offers an excellent opportunity for significant energy conservation, with all associated economic and environmental benefits, since although the conventional year-round residential comfort systems improve living standards, their use is responsible for significant energy consumption in the contemporary human society.

Appreciable amount of attention has already been given on the theoretical investigation of the transient thermal behavior of structural walls. Previous extensive research on the heat transfer analyses, has mostly been based on equivalent electrical network theory and numerical methods [1–5]. Since their effect is not completely independent of the thermal behavior of the rest of the building, this has also led to the development of extensive whole building analyses, as discussed by Rabl [6].

Although the construction with heavy external wall envelopes is a technological tradition in certain geographical regions of the world, the interest in the use of massive building envelopes not only remains still alive but grows worldwide. This is attributed to the ever growing energy efficiency concern, particularly in parallel with the need for increased utilization of passive solar design, owing to the possibilities of significant energy conservation and associated favorable environmental impacts.

It is believed however, that the thermal resistance or the wall U value as derived from simple steady-state

E-mail address: ptsiling@teiath.gr.

0360-1323/$ - see front matter © 2005 Elsevier Ltd. All rights reserved.
doi:10.1016/j.buildenv.2005.02.031

Nomenclature

A	area, m^2
C	heat capacity, J/K
c	specific heat capacity, J/kg K
HCA	per unit surface area heat capacity, J/m^2 K
h	convective heat transfer coefficient, W/m^2 K
I	incident solar radiation, W/m^2
K	numerical constant
k	thermal conductivity, W/mK
L	wall thickness, m
m	mass, kg
n	number of sublayer sections Δx
p	number of time increments Δt
q	heat flux rate, W/m^2
t	time, s
T	temperature, C
TC	time constant, s
U	overall heat transfer coefficient, U value, W/m^2 K
x	space coordinate, m

Greek letters

α	total hemispherical absorptivity, dimensionless
Δ	difference
δ	layer thickness, m
ρ	density, kg/m^3
φ	phase angle, deg.

Subscripts

av	average
c	concrete
ci	convective, room side
co	convective, ambient side
d	domain
F	forward
i	thermal insulation, node number
H	high heat capacity
L	low heat capacity
mw	mean value, winter
ms	mean value, summer
p	plaster
s	summer
r	room
ri	radiative, indoor surface
ro	radiative, outdoor surface
R	reverse
w	winter
∞	ambient

considerations [7], does not either accurately reflect the dynamic thermal performance or represent a reliable energy conservation indicator for walls. Walls with the same U value but different heat capacities exhibit a completely different thermal behavior, which physically leads to the slower wall response to imposed meteorological driving forces and improved long-term energy efficiency. The effect of heat capacity distribution has also sporadically been considered earlier in the literature [8,9], showing a rather insignificant effect on year around thermal behavior and long-term efficiency of structures.

The use of massive building envelope leads to reduction and phasing out of peak loads, something which can easily be quantified, by the definition of the wall damping-out efficiency factors, that were calculated for a broad range of typical walls by Tsilingiris [10]. The persistent interest in residential energy efficiency has also recently increased the popularity and marketing of various innovative structural products, suitable for the design and construction of the building envelope. Among these are the increased heat capacity steel frame walls, prefabricated concrete walls with a heavily insulated core and even PCM walls of greatly enhanced thermal capacity as discussed by Stovall and Tomlinson [11]. The main constraint for the wide acceptance of innovative walls is the lack of a widely accepted wall rating and evaluation method, or a realistic energy savings indicator for comparative evaluation of thermal performance and energy conservation.

It is clear that additional criteria are required to account for the effect of heat capacity and wall added thermal mass. Towards this aim new criteria, including various interfacial effects as well as the influence of wall heat capacity known as thermal mass benefit, are put forward for consideration, as noticed by Christian and Kosny [12], to allow product rating and possibly a wall label, which will inform the consumers about the energy cost implication of various products.

Towards the development of new evaluation criteria, it has recently been suggested that the transient wall response to a given step temperature change under well-defined initial and boundary conditions, may reveal a characteristic wall property, the wall thermal time constant, which is directly related not only to the wall heat capacity but also to its spatial distribution [13].

The aim of the present work is the theoretical investigation of the effects of heat capacity and its spatial distribution on the transient and quasi-steady state thermal behavior of structural walls under the influence of typical meteorological driving forces, corresponding to mild Mediterranean climatic

conditions. The present investigation is focused on the fundamental dynamic physical behavior of a clear wall section and ignores any two-dimensional effects corresponding to the presence of typical interfacial envelope details, like wall to wall corners, connections and fenestration, thermal shorts and metal studs. Towards this aim a comparative transient and quasi steady-state heat transfer analysis between two groups of equal thermal resistance although of different heat capacity walls is carried out, to investigate effects solely attributed to heat capacity and its spatial distribution.

2. The theoretical model

The development of the transient temperature field in a composite wall of large lateral dimensions compared to its thickness, with thermophysical properties k, ρ and c which are allowed to vary at a direction perpendicular to the wall plane, is described by the one-dimensional conduction heat transfer equation,

$$\frac{\partial}{\partial x}\left(k\,\frac{\partial T}{\partial x}\right)=\rho c\,\frac{\partial T}{\partial t}. \tag{1}$$

The coordinate system is located at the external wall surface of a thickness L, with the axis x normal to the wall plane. Assuming that the wall separates a room at the fixed indoor temperature T_r from the environment at the temperature $T_\infty(t)$, the boundary conditions of the problem are the following heat balance equations at both wall surfaces,

$$q(0,t)=\alpha I(t)+(h_{co}+h_{ro})[T_\infty(t)-T(0,t)] \tag{2}$$

and

$$q(L,t)=(h_{ci}+h_{ri})[T(L,t)-T_r], \tag{3}$$

where $q(0,t)$ and $q(L,t)$ are the time-dependent heat fluxes flowing at a direction perpendicular to the wall plane, and h_{co}, h_{ci} and h_{ri}, h_{ro} are the convective and radiative heat transfer coefficients for both the ambient and room wall sides respectively with α the wall total hemispherical absorbtivity for the ambient wall side.

The transient heat fluxes at both the wall sides are calculated by Fourrier's law,

$$q(0,t)=-k(\partial T/\partial x)|_{x=0}, \tag{4}$$

$$q(L,t)=-k(\partial T/\partial x)|_{x=L} \tag{5}$$

and the development of the numerical solution is based on the finite difference method.

Towards this aim the wall of thickness L is subdivided into n sublayer sections of thickness Δx so as $L=n\Delta x$. These sublayers are assumed to be isothermal with uniform thermophysical properties, at the centre of which a node of a thermal network is located. The entire time domain of integration t_d is also subdivided in a large number p of time increments Δt, so as $t_d=p\Delta t$. Expressions (1)–(3) were translated to a set of simultaneous algebraic equations, corresponding to each inner and boundary nodes of the thermal network, using the always inherently stable Laasonen implicit finite difference scheme [14,15]. Additional calculations based on the Crank–Nickolson finite difference approximation have always shown negligible difference between results. For the purpose of the present investigation, the thermal radiation effects were ignored $h_{ri}=h_{ro}=0$. Assuming that T_i^t denotes the temperature at the location of the thermal network node i at the time increment elapsed t and following the necessary algebraic manipulations, the derived equations for the inner i, where $2\leqslant i\leqslant n$, and the boundary nodes, 1 and $n+1$ of the thermal network are becoming respectively,

$$T_i^{t+1}\left(k_{i-1}+k_i+\frac{HC_i\Delta x^2}{\Delta t}\right)-k_{i-1}T_{i-1}^{t+1}-k_iT_{i+1}^{t+1}=\frac{HC_i\Delta x^2}{\Delta t}T_i^t, \tag{6}$$

$$T_1^{t+1}\left(h_{co}\Delta x+k_1+\frac{1}{2}\frac{\rho_1c_1\Delta x^2}{\Delta t}\right)-k_1T_2^{t+1}=\Delta xh_{co}T_\infty^{t+1}+\alpha I\Delta x+\frac{1}{2}\frac{\rho_1c_1\Delta x^2}{\Delta t}T_1^t, \tag{7}$$

$$T_{n+1}^{t+1}\left(k_n+h_{ci}\Delta x+\frac{1}{2}\frac{\rho_nc_n\Delta x^2}{\Delta t}\right)-k_nT_n^{t+1}=h_{ci}\Delta xT_i^{t+1}+\frac{1}{2}\frac{\rho_nc_n\Delta x^2}{\Delta t}T_{n+1}^t, \tag{8}$$

where $HC_i=\frac{1}{2}(\rho_{i-1}c_{i-1}+\rho_ic_i)$. The above Eqs. (6)–(8) were employed to develop the matrix equation of the problem. The solution of the set of the developed $n+1$ simultaneous algebraic equations during each time increment of the time domain t_d, which corresponds to p simulation steps was carried out numerically in a digital microcomputer, using the triangular factorization method.

The accuracy of numerical solution improves as the number of sublayer sections and time increments Δx and Δt respectively increase, so as the selection of the optimum number of sublayer sections, which determines the number of the thermal network nodes and the time step, is a trade-off between computer CPU time and desired accuracy level of calculations. This selection which was based on extensive numerical experiments, corresponds usually to a sublayer thickness of 1 cm and a time step between 60 and 300 s, as it was also discussed in [5]. The developed numerical model was successfully evaluated against analytical solutions from the theory [10].

The instantaneous values of incident solar radiation and ambient temperature which appear in expressions (2) and (7), represent the periodic meteorological time-dependent forcing functions to the boundary conditions

of the problem. Derivation of instantaneous values of the incident solar radiation is based on existing long-term, statistically treated sample of some 25 years of solar radiation measurements from the National Observatory of Athens for the period 1961–1980, which were integrated over all hours of the day to derive average daily values of incident solar radiation in a horizontal plane by Kouremenos et al. [16]. The derived long-term statistically treated daily average data are employed to derive corresponding hourly values of solar insolation, incident at a vertical south faced plane, according to the well established procedures described by Duffie and Beckmann [17] as also discussed by Tsilingiris in [18]. The necessary instantaneous values of incident solar radiation at the vertical south-faced wall in w/m^2 for winter and summer simulations starting at the 20th day of January or July respectively, were derived by the following simple polynomial fit expressions of the derived hourly data, valid for the sunshine hours of the day,

$$I_w(t) = K_{w1} + K_{w2}t + K_{w3}t^2 + K_{w4}t^3 + K_{w5}t^4, \tag{9}$$

$$I_s(t) = K_{s1} + K_{s2}t + K_{s3}t^2 + K_{s4}t^3 + K_{s5}t^4, \tag{10}$$

where t the time in hours from the midnight and K_{wi} and K_{si}, $i = 1-5$, numerical constants for the winter and summer data, with typical values for the 20th day of January and July, $K_{w1} = 1463.74$, $K_{w2} = -897.912$, $K_{w3} = 157.295$, $K_{w4} = -9.99013$, $K_{w5} = 0.208128$ and $K_{s1} = 2033.53$, $K_{s2} = -1024.92$, $K_{s3} = 170.03$, $K_{s4} = -10.6104$, $K_{s5} = 0.221051$, respectively.

The calculation of the instantaneous values of the employed ambient temperature is based on existing long-term daily range, maximum and average temperatures for each day of the year for Athens, which were derived by statistical treatment of long-term temperature measurements during the period 1950–1975. These data were fitted with a good accuracy by harmonic functions by Kouremenos and Antonopoulos [19] and were employed for the calculation of the hourly average of ambient temperature throughout the day, according to the model proposed by ASHRAE [20]. For the purpose of the present winter and summer simulations, the derived hourly data were fitted with a good accuracy by the following simple harmonic functions:

$$T_{\infty w}(t) = \bar{T}_w + T_{mw}\cos\left(\frac{2\pi}{24}t - \varphi_w\right), \tag{11}$$

$$T_{\infty s}(t) = \bar{T}_s + T_{ms}\cos\left(\frac{2\pi}{24}t - \varphi_s\right), \tag{12}$$

with typical mean and amplitude values for the 20th January and July $\bar{T}_w = 8.62\,^\circ C$, $T_{mw} = 3.68\,^\circ C$ and $\bar{T}_s = 26.51\,^\circ C$, $T_{ms} = 6.2\,^\circ C$ respectively, and phase angle $\varphi_w = \varphi_s = 225^\circ$.

3. The distribution of wall layer heat capacity

Although the effect of layering low thermal conductivity materials in a composite wall contributes the wall thermal resistance, it also leads to the increase of wall heat capacity.

The heat capacity is an important property that enables walls to absorb, store and release at a later time energy in the building space. This quantity combined to the wall thermal resistance, is responsible for significant peak load suppression and phasing out as well as long-term energy efficiency improvement, known as wall mass effect [12]. The heat capacity of a composite wall with n sublayers of a specific heat capacity c_i is

$$C = \sum_{i=1}^{n} m_i c_i. \tag{13}$$

More frequently instead of the previous quantity, the per unit wall surface area heat capacity ($J/m^2\,K$) is employed, defined as

$$HCA = C/A = \sum_{i=1}^{n} \rho_i c_i \delta_i, \tag{14}$$

where ρ_i and δ_i the wall sublayer density and thickness respectively.

The definition of a new wall dynamic physical quantity, the wall thermal time constant, has been recently proposed [13], to quantify how rapidly an isothermal wall at thermal equilibrium responds to a properly defined step temperature change, imposed at a particular wall side. This quantity is broadly employed in physics to describe the transient response characteristics of systems under the influence of a step change of a particular parameter. For an isothermal wall in thermal equilibrium, which at $t = t_o$ is exposed in a step temperature change at its ambient side, it can be evaluated by the numerical solution of Eq. (1) under the following boundary conditions:

$$-k(\partial T/\partial x)|_{x=0} = h[T_s(t) - T(0,t)] \tag{15}$$

and

$$-k(\partial T/\partial x)|_{x=L} = h[T(L,t) - T_r], \tag{16}$$

where $h = 12\,W/m^2\,K$ the convective heat transfer coefficients, which are assumed to be identical at both wall sides, with

$$T_s(t) = \begin{cases} 0, & \text{for } t < t_o, \\ T_s, & \text{for } t \geqslant t_o. \end{cases} \tag{17}$$

The transient thermal behavior of a given composite wall structure under the influence of imposed temperature gradients, depends strongly on the wall heat capacity, which although lacking any directional significance, is closely related to the wall thermal time constant.

It was found that the wall thermal time constant has strongly directional characteristics, related to the specific wall side. This leads to the definition of the forward $(TC)_F$, and reverse $(TC)_R$ time constant, which are generally not equal. Assuming deliberately that the forward time constant is the one derived under the assumption that a step temperature change is developed at the room wall side, the reverse time constant is respectively defined as the one derived by the development of an identical time step at the ambient wall side. The definition of these two different quantities is attributed to the uneven distribution of heat capacity at a direction perpendicular to the wall plane. Therefore multilayer structures with thick layers of dense materials with large heat capacity close to the room side, correspond to a high forward and a low reverse wall time constant values, so as $[(TC)_F/(TC)_R]>1$, otherwise $[(TC)_F/(TC)_R]<1$. Assuming that convective heat transfer coefficients are identical, the symmetrical distribution of heat capacity relatively to the wall plane of symmetry leads to identical forward and reverse time constants so as $[(TC)_F/(TC)_R]=1$.

The calculation of the thermal time constant for a group of various typical multilayer wall structures usually employed in construction, has shown that the $(TC)_F/(TC)_R$ ratio may considerably vary, with the exception of the symmetrical walls with a unity thermal time constant ratio [13].

4. The analysis and description of wall samples

The present investigation is based on the comparative thermal behavior analysis between two wall groups. The first group includes basic lightweight panel walls, while the second is comprised of heavier thermally insulated

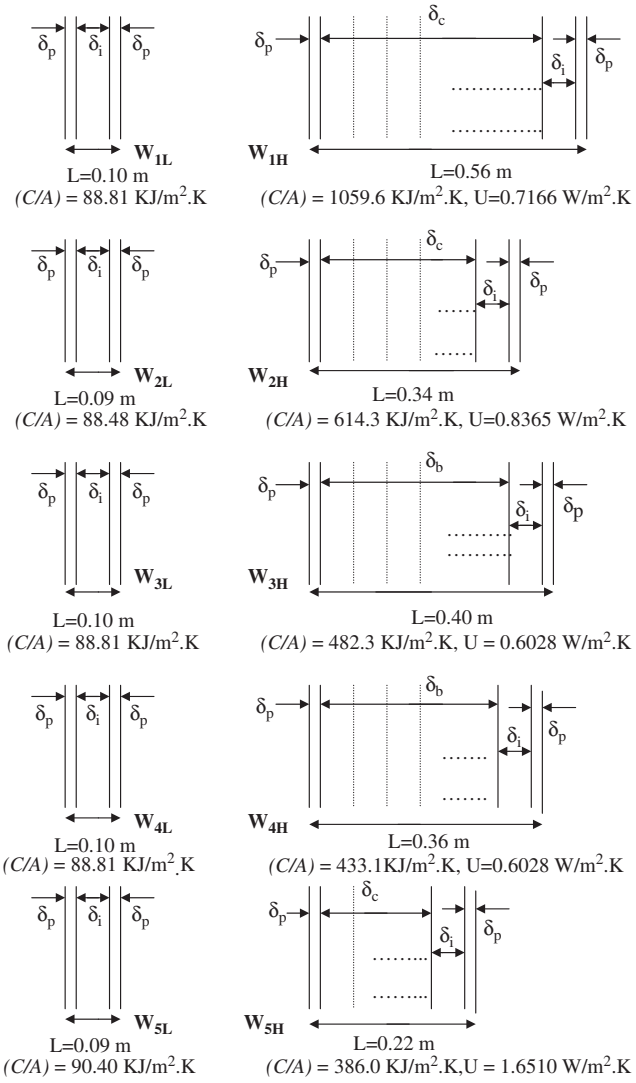

Fig. 1. The design description of the lightweight wall panel group, walls W_{1L} to W_{5L}, as compared to the equal thermal resistance although heavier walls W_{1H} to W_{5H}. The thickness L, the HCA and the U value of wall pairs, are also shown. The indicated sublayer thicknesses and thermophysical properties are shown in Table 1.

Table 1
Per unit area heat capacity, U value, sublayer thicknesses and thermophysical properties of lightweight (L) and large heat capacity (H) walls W_1–W_5

Wall type	W_{1L}	W_{1H}	W_{2L}	W_{2H}	W_{3L}	W_{3H}	W_{4L}	W_{4H}	W_{5L}	W_{5H}
U (W/m^2 K)	0 .7166		0.8365		0.6028		0.6028		1.6510	
HCA (KJ/m^2 K)	88.81	1059.6	88.48	614.3	88.81	482.3	88.81	433.1	90.4	386
δ_i (m)	0.06	0.04	0.05	0.04	0.06	0.04	0.06	0.04	0.05	0.04
k_i (W/m K)	0.05	0.05	0.05	0.05	0.041	0.041	0.041	0.041	0.0729	0.0729
ρ_i (kg/m^3)	40	40	40	40	40	40	40	40	60	60
c_i (J/kg K)	840	840	840	840	840	840	840	840	880	880
δ (m)	–	0.48	–	0.26	–	0.32	–	0.28	–	0.14
k (W/m K)	–	1.20	–	1.30	–	0.656	–	0.574	–	1.70
ρ (kg/m^3)	–	2300	–	2300	–	1400	–	1400	–	2300
c (J/kg K)	–	880	–	880	–	880	–	880	–	920

All plaster layers are $\delta_p = 0.02$ m with $k_p = 1.39$ W/m K, $\rho_p = 2000$ kg/m^3 and $c_p = 1085$ J/Kg K.

multilayer walls of appreciably higher heat capacity although of equal thermal resistance. The requirement of equal thermal resistance (or identical U value) as derived from simple steady-state considerations between the two wall groups, was imposed in order to allow the investigation of effects solely attributed to the wall heat capacity. Proper selection of sublayer thicknesses and thermal conductivities has allowed the definition of pairs of lightweight panels and massive walls of identical U value.

The design description of the lightweight wall panel group, walls W_{1L} to W_{5L}, is shown in Fig. 1 as compared to the heavier wall designs W_{1H} to W_{5H} of the same thermal resistance. In the same figure the wall thickness L, the identical U value of wall pairs as well as the per unit wall surface area heat capacity HCA, are also shown. Thicknesses and thermophysical properties of the wall sublayers are shown in Table 1. From a direct inspection of the thermophysical properties, it is derived that W_{1H} and W_{2H} may correspond to walls with a reinforced concrete layer of any possible composition to match the numerical values of density and thermal conductivity shown in Table 1, while W_{3H} and W_{4H} to walls with a brick layer of any specification or air void fraction, to match the corresponding thermophysical properties. The wall W_{5H} with a thermal conductivity of 1.70 W/m^2 K can possibly represent a thermally insulated, heavily reinforced concrete structure.

As shown in Fig. 1, although the per unit area heat capacity for the first group of lightweight wall panels is around 90 KJ/m^2 K, the corresponding quantity for the second heavier wall group is appreciably higher and has been allowed to vary within a remarkably wide range between 1059.6 and 386 KJ/m^2 K.

For the investigation of the effects of the spatial distribution of heat capacity on the transient and quasi steady-state thermal behavior of the heavy multi-layer walls of the second group, the thermal insulation layer was allowed to move from the room to the ambient side, at a direction perpendicular to the wall plane.

Since heat capacity distribution is closely associated to the wall thermal time constant, this leads to a forward thermal time constant increase within a wide range between a minimum and a maximum value, leading to a corresponding decrease of $(TC)_F/(TC)_R$ ratio, while the wall thermal resistance remains unchanged.

Typical results for the walls W_{1H}, W_{3H} and W_{4H} corresponding to a HCA of 1059.6, 482.3 and 433.1 KJ/m^2 K respectively are presented in Table 2, which shows the calculated values of $(TC)_F$, $(TC)_R$ and $(TC)_F/(TC)_R$ ratio as the thermal insulation layer moves from the room to ambient side. The whole 0.52 m interior wall section of the wall W_{1H} with $L = 0.56$ m, was splited into 13 zones of 4 cm thickness, the first being the one placed closely to the room while the 13th closely to the ambient wall side, underneath the plaster layer. A thermal insulation layer of 4 cm thick was allowed to move successively from the location 1, which is close to the room side, to location 13 at the opposite

Table 2
Calculated values of forward $(TC)_F$, reverse $(TC)_R$ time constants and $(TC)_F/(TC)_R$ ratio based on $h_{ci} = h_{co} = h_c = 12\,W/m^2\,K$, for the walls W_{4H}, W_{3H} and W_{1H}

Wall W_{4H}: $(C/A) = 433.1\,KJ/m^2\,K$							
Zone number	1	3	6	8			
$(TC)_F$ (h)	1.18	3.00	3.32	3.33			
$(TC)_R$ (h)	3.33	3.32	3.00	1.18			
$(TC)_F/(TC)_R$ (-)	0.354	0.903	1.106	2.822			
Wall W_{3H}: $(C/A) = 482.3\,KJ/m^2\,K$							
Zone number	1	3	5	7	9		
$(TC)_F$ (h)	1.155	3.06	3.58	3.60	3.60		
$(TC)_R$ (h)	3.60	3.60	3.58	3.06	1.155		
$(TC)_F/(TC)_R$ (-)	0.320	0.85	1.00	1.176	3.116		
Wall W_{1H}: $(C/A) = 1059.6\,KJ/m^2\,K$							
Zone number	1	3	5	7	9	11	13
$(TC)_F$ (h)	1.12	4.55	6.62	7.25	7.33	7.33	7.33
$(TC)_R$ (h)	7.33	7.33	7.33	7.25	6.62	4.55	1.12
$(TC)_F/(TC)_R$ (-)	0.152	0.620	0.903	1.00	1.107	1.610	6.544

side in 8 cm steps, thus developing seven different walls W_{1Hj}, $j = 1-7$, of identical thickness and U value, although of different forward and reverse time constants.

In a similar way the walls W_{3H} and W_{4H} were also subdivided into nine and eight different zones respectively, and the time constants of the five W_{3Hj}, $j = 1-5$, and the four developed walls W_{4Hj}, $j = 1-4$ respectively, of uniform U value are also shown in Table 2. The calculated forward time constant was plotted against the reverse time constant for the three typical walls W_{1H}, W_{3H} and W_{4H} in Fig. 2. Along with the appreciably higher time constants for the wall W_{1H}, it can also be seen that as the thermal insulation layer moves towards the ambient wall side, the forward time constant increases while the reverse time constant decreases. This effect is attributed to the redistribution of heat capacity normally to the wall plane, which being initially located closely to the ambient wall surface, it moves towards the room side as the thermal insulation layer moves towards the opposite side. Since $h_{ci} = h_{co} = h$, the data points in Fig. 2 are symmetrically distributed within the broken diagonal unity line $(TC)_F/(TC)_R = 1$, owing to the development of equal values of forward and reverse time constant, when the thermal insulation layer is placed at symmetrically located zones in respect to the wall plane of symmetry. The data points corresponding to zones 7 and 5 for the walls W_{1H} and W_{3H} respectively are lying on the unity slope diagonal line. This is attributed to the fact that the plane of symmetry of these zones is identical to the plane of symmetry of the corresponding walls, which leads to identical forward and reverse time constants.

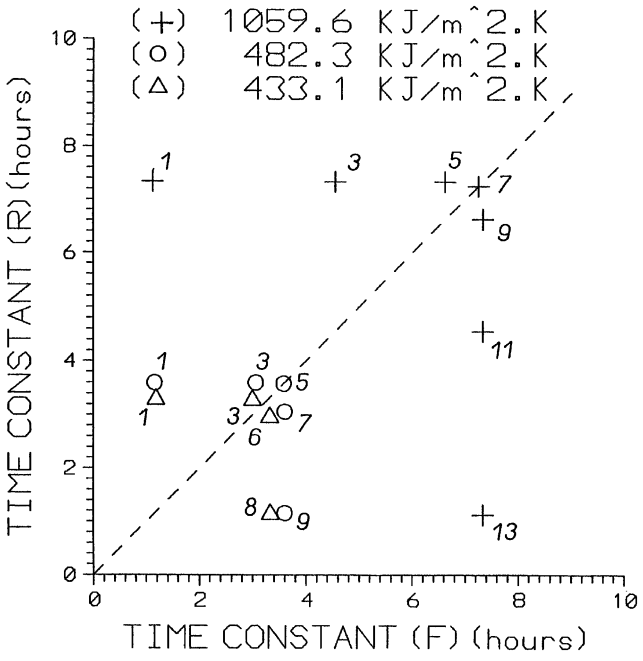

Fig. 2. Forward versus reverse thermal time constant plot for the $W_{1H}(+)$, $W_{3H}(o)$ and $W_{4H}(\triangle)$ walls. Data point numbers correspond to the respective zone number of the 4 cm thick thermal insulation layer, starting from the ambient wall side. Walls $W_{1H,7}$ and $W_{3H,5}$ are completely balanced with equal forward and reverse time constants.

5. Results and discussion

The derived numerical solution of Eq. (1) under the appropriate boundary conditions 2,3, allowed the calculation of the time dependent heat flux for all the lightweight panel W_{1L} to W_{5L} and the heavy walls W_{1H} to W_{5H}. Both the winter and summer simulations, were

carried out during the time domain of five sequential days starting at the 20th day of January and July respectively, although it was necessary to carry out additional even longer simulation runs particularly for the W_{1H} wall, because of its excessively high heat capacity. The developed transient wall temperature field is responsible for the corresponding development of transient heat fluxes, which asymptotically converge to their periodically time-varying values.

For the simulations carried out under winter conditions, the walls are assumed to be initially isothermal, at the uniform temperature of 15 °C. It is also assumed that the room space at the fixed temperature of 20 °C, exchanges heat with the environment through the wall, the ambient side of which is subjected to the effect of the time dependent meteorological driving forces. For summer conditions, the walls are assumed to be at the initial uniform temperature of 25 °C, while the fixed room temperature is maintained at 26 °C. The influence of the absorption of the incident solar radiation on the surface of a south-faced wall was investigated, by assuming the effect of an either completely shaded ($\alpha = 0$) or a sunlit wall with $\alpha = 0.5$.

The calculated time dependent heat fluxes $q_{iL}(t)$ and $q_{iHj}(t)$ were comparatively plotted for the two groups of the corresponding walls W_{iL} and W_{iHj}, $i = 1-5$ respectively, of uniform U value, although different HCA ratio. The results were organized to cover meteorological conditions corresponding to both winter and summer loads.

Typical results for the walls W_{3L} and W_{3Hj} of a uniform $U = 0.6028\,\mathrm{W/m^2\,K}$, corresponding to $(\mathrm{HCA})_L = 88.81$ and $(\mathrm{HCA})_H = 482.3\,\mathrm{KJ/m^2\,K}$ respectively, are presented in Figs. 3–6, in which also the incident solar radiation and ambient temperature are also plotted in dotted and broken lines respectively. In Fig. 3, which corresponds to the derived results for the completely shaded walls subjected to winter meteorological conditions, the heat flux $q_{3L}(t)$ as calculated by Eq. (3) was plotted as a function of time for the lightweight panel wall W_{3L} of $(\mathrm{HCA})_L = 88.81\,\mathrm{KJ/m^2\,K}$ by curve (1). In the same plot the quantities $q_{3H1}(t)$, $q_{3H2}(t)$ to $q_{3H5}(t)$, corresponding to the five walls of uniform $(\mathrm{HCA})_H$ and U values, although of increasing forward time constant as the thermal insulation layer moves from the room to the ambient wall side in 8 cm steps, are comparatively plotted as a function of time by curves 2–6.

It can be seen that following a very short transient, typically lasting about 24 h during which maximum negative transient heat fluxes (heat losses) as high as $55\,\mathrm{W/m^2}$ occur, the time dependent heat flux for the lightweight panel wall W_{3L} approaches its harmonically time varying value.

At the same time the thermal behavior of the heavier walls W_{3H1}, W_{3H2} to W_{3H5} of increasing forward time constant (curves 2–6) is completely different. Quasi steady-state time-varying periodic solutions are asymptotically approached after a significantly longer transient, which

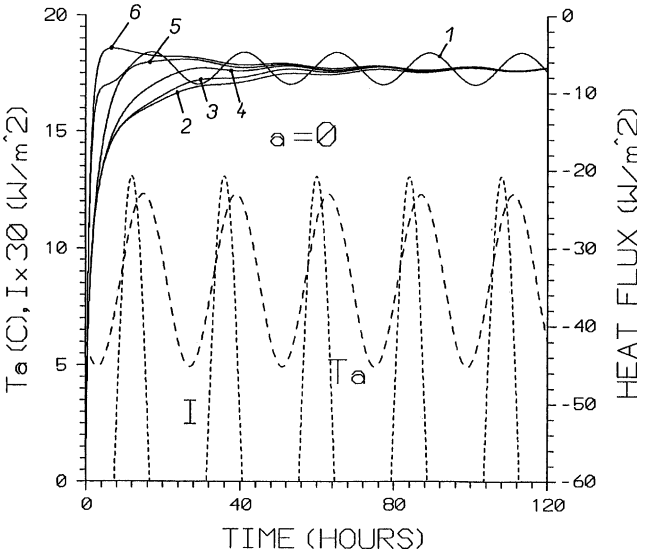

Fig. 3. The time dependent heat flux for the uniform U value walls W_{3L} and W_{3Hj} of $U = 0.6028\,\mathrm{W/m^2\,K}$. Curve 1 corresponds to W_{3L} wall of $(\mathrm{HCA})_L = 88.81\,\mathrm{KJ/m^2\,K}$ while curves 2–6 correspond to the W_{3Hj}, $j = 1-5$ walls of $(\mathrm{HCA})_H = 482.3\,\mathrm{KJ/m^2\,K}$. The presented results are based on simulations which were carried out during five successive winter days, starting on the 20th of January for a south-faced wall with $\alpha = 0$. Solar insolation (I) and ambient temperature (T_a) are also shown in dotted and broken lines, respectively.

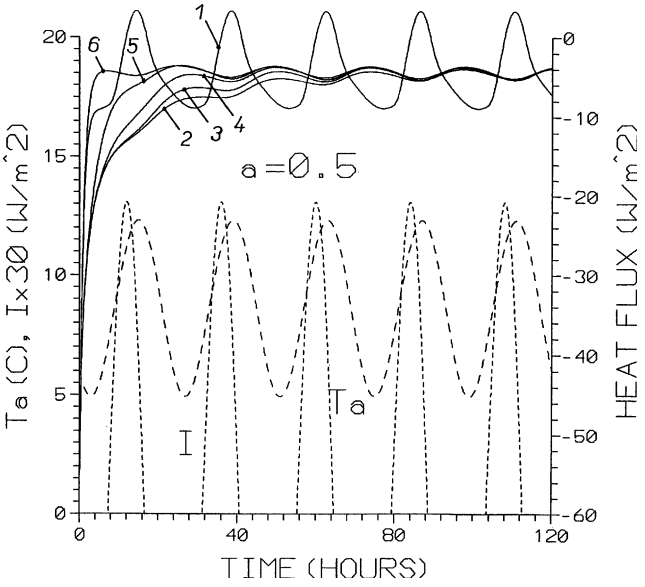

Fig. 4. The time dependent heat flux for the same walls W_{3L} and W_{3Hj} as in Fig. 3. Curve 1 corresponds to W_{3L} wall of $(\mathrm{HCA})_L = 88.81\,\mathrm{KJ/m^2\,K}$ while curves 2–6 correspond to the W_{3Hj}, $j = 1-5$ walls of $(\mathrm{HCA})_H = 482.3\,\mathrm{KJ/m^2\,K}$. The presented results are based on simulations carried out during five successive winter days starting on the 20th of January for a south-faced wall with $\alpha = 0.5$. Solar insolation (I) and ambient temperature (T_a) are also shown in dotted and broken lines, respectively.

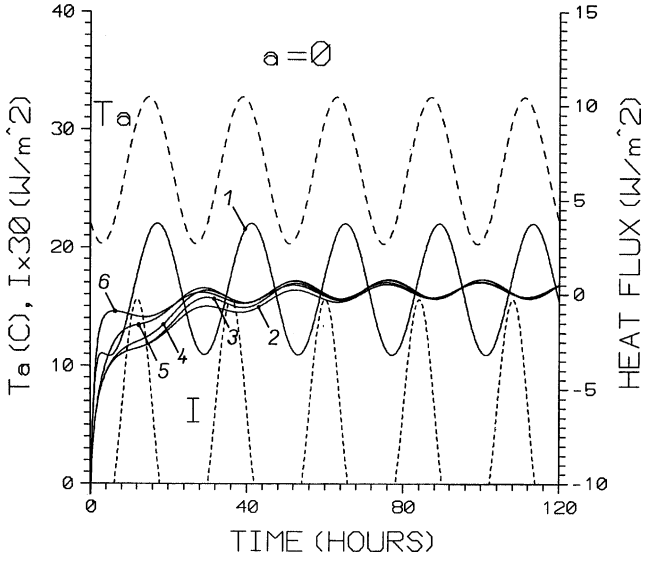

Fig. 5. The time dependent heat flux for the same walls as in Fig. 3, based on simulations carried out during five successive summer days starting on the 20th of July for a south-faced wall with $\alpha = 0$. Solar insolation (I) and ambient temperature (T_a) are also shown in dotted and broken lines, respectively.

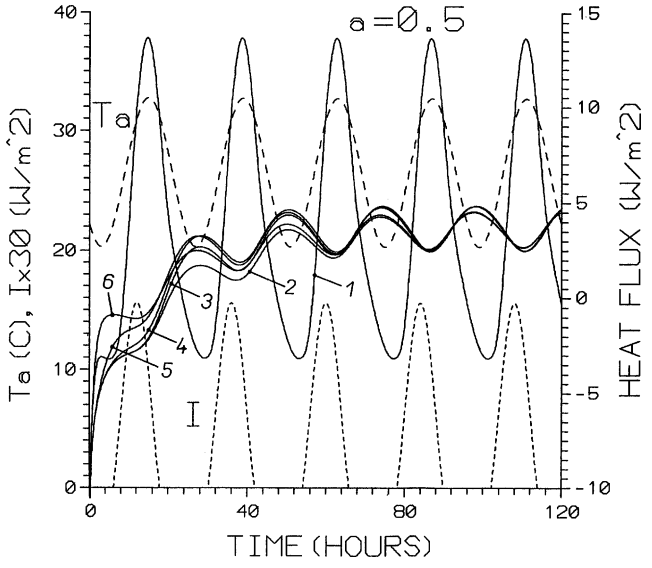

Fig. 6. The time dependent heat flux for the same walls as in Fig. 3, based on simulations carried out during five successive summer days starting on the 20th of July for a south-faced wall with $\alpha = 0.5$. Solar insolation (I) and ambient temperature (T_a) are also shown in dotted and broken lines, respectively.

typically lasts more than 80 h, during which appreciably high transient heat fluxes occur. As can be seen from comparing curves 1–6, although the time dependent quasi steady-state solutions for these heavy walls develop identical average values to those corresponding to panel wall W_{3L}, they appreciably differ in the way they asymptotically approach the quasi steady-state periodic behavior, during the development of the transient.

The average value of periodic quasi steady-state winter heat fluxes $\bar{q}_{3L|w}$ and $\bar{q}_{3Hj|w}$ for the lightweight wall W_{3L} and the five walls W_{3Hj}, $j = 1-5$, of uniform U value was calculated by the following expressions:

$$\bar{q}_{3L|w} = [1/(t_2 - t_1)] \int_{t_1}^{t_2} q_{3L}(t)|_w \, dt, \tag{18}$$

$$\bar{q}_{3Hj|w} = [1/(t_2 - t_1)] \int_{t_1}^{t_2} q_{3Hj}(t)|_w \, dt, \tag{19}$$

where the integration limits are $t_1 = 96$ and $t_2 = 120$ h, which correspond to an average calculated value for the fifth simulation day when all transients have died away for all the walls except W_{1Hj}. It was found that the calculated average values $\bar{q}_{3H1|w}$ to $\bar{q}_{3H5|w}$ from expression (19) corresponding to the uniform (HCA) $= 482.3\,\mathrm{KJ/m^2\,K}$ are spread around $6.9\,\mathrm{W/m^2}$ typically within a 1% range. This is confirmed by a direct inspection of curves 2–6 in Fig. 3 corresponding to the time depended heat fluxes $q_{3H1}(t)|_w$ to $q_{3H5}(t)|_w$, which are becoming identical for the fifth simulation day. It was also found that the quasi steady-state heat flux for the wall W_{3L} as derived from expression (18) is within about 1% identical to the corresponding heat flux for all the walls W_{3Hj} as derived from expression (19), so as,

$$\bar{q}_{3L|w} = \bar{q}_{3Hj|w} \tag{20}$$

for $j = 1-5$. This can also be confirmed by the comparative inspection of the heat flux curve 1 with curves 2–6, all of which develop during the fifth simulation day an identical average value. This value is equal to the corresponding heat flux as predicted according to simple steady-state considerations,

$$\bar{q} = U(T_{av} - T_r), \tag{21}$$

where $T_{av} = 8.62\,^{\circ}\mathrm{C}$ is the daily average ambient temperature and $U = 0.6028\,\mathrm{W/m^2\,K}$. It can also be seen that the significant increase of the wall HCA from the value of 88.81 to $482.30\,\mathrm{KJ/m^2\,K}$, leads in addition to a considerable suppression, also to a significant phasing out of the developed wall peak heat flux.

There is also a dramatic effect of spatial distribution of heat capacity on the transient wall thermal behavior as derived from Fig. 3. When the thermal insulation layer of low heat capacity is located at the ambient wall side, the wall layers of large heat capacity are distributed closely to the room wall side. This leads to a maximum forward wall thermal time constant and a lengthy transient response with an appreciably slow asymptotic approach to the corresponding periodically time-varying heat flux, as can be seen from curve 2.

As the thermal insulation layer moves towards room side, redistribution of heat capacity leads to a forward time constant reduction. Symmetric distribution of heat capacity occurs when the thermal insulation layer is at the wall mid-plane (curve 4), something which leads to

identical forward and reverse time constants. Further displacement of thermal insulation leads to a minimum forward and maximum reverse time constant, when the thermal insulation layer is at the room side underneath the plaster layer (curve 6).

The transient time dependent heat flux curves for all the walls of different distribution of heat capacity tend to approach each other and to become eventually identical at around 100 h when all transients have died away. From this time onwards there is completely no effect of the spatial distribution of heat capacity on the quasi steady-state periodic behavior and wall average heat flux.

The influence of absorption of the incident solar radiation during the same period of winter simulations can be seen in Fig. 4, in which the comparative effect of a total hemispherical absorptivity of $\alpha = 0.5$ can be seen on the transient and quasi steady-state wall thermal behavior. As derived from curve 1, strong radiation absorption at the lightweight panel wall surface W_{3L} causes a significant reduction of heat flux, which shortly after midday when the maximum incident solar radiation and ambient temperature occur becomes positive (heat gain). This is attributed to the significant reduction of the transient temperature gradients at the ambient wall side. It is also worth noting the remarkably short transient for the wall W_{3L} owing to its low heat capacity, before the development of the periodic quasi steady-state behavior. This behavior corresponds to a larger time-depended heat flux amplitude, although of a significantly lower average value of about 4.5 W/m^2.

Calculation of the average quasi steady-state heat flux through expressions (18) to (19) for the sunlit walls with an $a = 0.5$, have also confirmed the validity of expression (20) for simulations corresponding to winter conditions.

The quasi steady-state summer average heat fluxes $\bar{q}_{3L|s}$ and $\bar{q}_{3Hj|s}$ for the lightweight wall W_{3L} and the five walls W_{3Hj}, $j = 1-5$ of increasing forward time constant respectively, were subsequently calculated by the corresponding expressions:

$$\bar{q}_{3L|s} = [1/(t_2 - t_1)] \int_{t_1}^{t_2} q_{3L}(t)|_s \, dt, \tag{22}$$

$$\bar{q}_{3Hj|s} = [1/(t_2 - t_1)] \int_{t_1}^{t_2} q_{3Hj}(t)|_s \, dt, \tag{23}$$

with the same integration limits corresponding to the fifth simulation day. Calculated results have shown that the average summer values $\bar{q}_{3H1|s}$ to $\bar{q}_{3H5|s}$ from expression (23) were identical, something which is confirmed by the inspection of curves 2–6 corresponding to $q_{3H1}(t)|_s$ to $q_{3H5}(t)|_s$, which are becoming identical for the fifth simulation day, as can be seen from Figs. 5 and 6. The quasi steady-state heat flux as derived from expression (22) is also within less than 1% identical to the corresponding heat flux derived from expression (23), for all the five walls W_{3H1} to W_{3H5} of uniform HCA and U value although of a different forward time constant, so as,

$$\bar{q}_{3L|s} = \bar{q}_{3Hj|s}, \tag{24}$$

for $j = 1-5$. This can also be confirmed by the inspection of curves 1–6, which appear to develop identical average values during the fifth simulation day.

Presentation of results corresponding to the calculated average heat flux for all the walls W_{iL} and W_{iHj}, $i = 1-5$, as derived from the simulations carried out during the prescribed period of five winter sequential days, are presented in Fig. 7.

In this plot the calculated quasi steady-state winter average heat flux $\bar{q}_{iL|w}$, $i = 1-5$, through expression (18) for a per unit area heat capacity of around 88 $KJ/m^2 K$ is presented against the quantity $\bar{q}_{iHj|w}$, which was derived through expression (19) for all the five walls W_{iHj} of a given HCA, ranging between 1059.6 and 386 $KJ/m^2 K$ for the j heat capacity distribution.

It can be seen that for a calculated $\bar{q}_{iL|w}$ value, the corresponding quasi steady-state heat fluxes $\bar{q}_{iH1|w}$, $\bar{q}_{iH2|w}$ to $\bar{q}_{iHj|w}$ are almost identical, especially for the relatively low heat capacity walls, of a per unit area heat capacity lower than about 600 $KJ/m^2 K$. For the walls of very large heat capacity, there is a scatter of the calculated data around the unity slope line. This is typically shown by the data corresponding to the large heat capacity wall of HCA = 1059.6 $KJ/m^2 K$, which leads to a considerably lengthy transient before the asymptotic approach to quasi steady-state conditions,

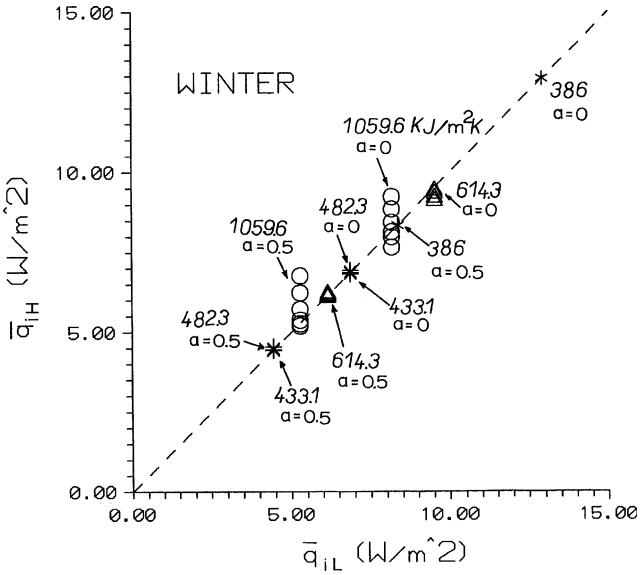

Fig. 7. Comparative presentation of the calculated average values of time dependent quasi steady-state heat flux $\bar{q}_{iHj}$ for the high heat capacity walls W_{iHj}, $i = 1-5$, plotted against the corresponding values $\bar{q}_{iL}$ for the low heat capacity walls W_{iL}, $i = 1-5$ as derived for the winter simulations and for $\alpha = 0$ or 0.5.

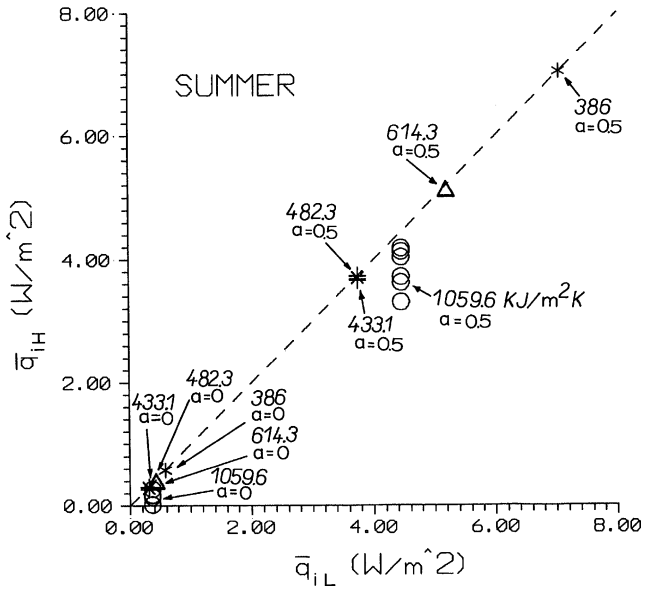

Fig. 8. Comparative presentation of the calculated average values of time dependent quasi steady-state heat flux $\bar{q}_{iHj}$ for the high heat capacity walls $W_{iHj}, i = 1-5$, plotted against the corresponding values $\bar{q}_{iL}$ for the low heat capacity walls $W_{iL}, i = 1-5$ as derived for the summer simulations and for $\alpha = 0$ or 0.5.

something which occurs far later than the prescribed period of 120 h time. Subsequent longer simulation runs for 240 h specifically for this wall have confirmed, that the calculated quasi steady-state heat flux becomes almost identical to the corresponding quantity for the lightweight panel wall of equal U value. This leads to a negligible scattering of $\bar{q}_{1Hj}$, $j = 1-7$ data, around the unity slope diagonal line.

The respective results for summer simulations are shown in Fig. 8, in which the derived lower average heat fluxes are attributed to the corresponding lower average temperature differences during summer. Again the plotted data points derived for a simulation time domain of 120 h appear on the unity slope line, confirming once more the validity of Eq. (24) for all the walls with a HCA ratio lower than about 600 KJ/m^2 K, with the exception of the scattered data points for HCA = 1059.6 KJ/m^2 K, which is also attributed to the excessively large heat capacity of the 1059.6 KJ/m^2 K wall. This scatter becomes negligible when the results correspond to subsequent longer simulation runs.

6. Conclusions

An analysis was carried out for the investigation of the effects of the heat capacity on the transient and quasi steady-state wall heat flux under the effect of harmonically time-varying meteorological driving functions. This analysis has allowed the calculation of the time dependent heat flux and its quasi steady-state average value, which may correspond to heat gain or loss into conditioned space, depending on summer or winter weather conditions. The investigation of effects, specifically attributed to heat capacity was made possible, by the proper design selection of uniform thermal resistance although of different heat capacity walls, ranging more than an order of magnitude. According to the results of extensive simulations and as far as the fundamental physical behavior of a clear wall section is concerned, it was derived that although the spatial distribution of heat capacity at a direction perpendicular to the wall plane strongly influences the transient wall heat flux and the asymptotic approach to the quasi steady-state periodic behavior, it has completely no effect on the time-average quasi steady-state wall heat flux. This happens irrespective of the wall heat capacity, season of the year leading either to winter heat loss or summer heat gain, meteorological parameters, incident solar radiation intensity at the ambient wall side and total hemispherical absorptivity of the wall surface.

References

[1] Maloney J, Wang Tseng-Chan, Chen Bing, Thorp J. Thermal network predictions of the daily temperature fluctuations in a direct gain room. Solar Energy 1982;29(3):207–23.
[2] Duffin RJ, Knowles G. A passive wall design to minimise building temperature swings. Solar Energy 1984;33(3/4):337–42.
[3] Haghighat F, Unny TE, Chandrashekar M. Stochastic modelling of transient heat flow through walls. ASME Journal of Solar Energy Engineering 1985;107:202–7.
[4] Athienitis AK, Sullivan HF, Hollands KGT. Analytical model, sensitivity analysis and algorithm for temperature swings in direct gain rooms. Solar Energy 1986;36(4):303–12.
[5] Tsilingiris PT. On the transient thermal behavior of structural walls—the combined effect of time-varying solar radiation and ambient temperature. Renewable Energy 2002;27:319–36.
[6] Rabl A. Parameter estimation in buildings: methods for dynamic analysis of measured energy use. ASME. Journal of Solar Energy Engineering 1988;110:2–66.
[7] European Standard CEN/EN 1934, Thermal performance of buildings-Determination of thermal resistance by hot box method using heat flow meter—Masonry, March 1998.
[8] Goodwin SE, Catani MJ. The effect of mass on heating and cooling loads and on insulation requirements of buildings in different climates. Transactions of ASHRAE part 1 1979: 869–84.
[9] Kossecka E, Kosny J. Relations between structural and dynamic thermal characteristics of building walls. Proceedings of 1996 International Symposium of CIBW67 "Energy and Mass Flow in the life cycle of Buildings", Vienna, 4–10 August 1996. p. 627–32.
[10] Tsilingiris PT. Thermal flywheel effects on the time varying conduction heat transfer through structural walls. Energy and Buildings 2003;35:1037–47.
[11] Stovall TK, Tomlinson JJ. What are the potential benefits of including latent storage in common wallboard? ASME. Journal of Solar Energy Engineering 1995;117:318–25.
[12] Christian JE, Kosny J. Thermal performance and wall ratings. ASHRAE Journal 1996;56–65.
[13] Tsilingiris PT. On the thermal time constant of structural walls. Applied Thermal Engineering 2004;24:743–57.

[14] Richtmeyer RD. Difference methods for initial-value problems. New York: Interscience Publication; 1957.
[15] Croft DR, Lilley DG. Heat transfer calculations using finite difference equations. London: Applied Science Publishers; 1977.
[16] Kouremenos DA, Antonopoulos KA, Domazakis ES. Solar radiation correlations for Athens, Greece Area. Solar Energy 1985;35:259–69.
[17] Duffie JA, Beckmann WA. Solar engineering of thermal processes. New York: Wiley; 1980.
[18] Tsilingiris PT. Solar water heating design—a new simplified dynamic approach. Solar Energy 1996;57(1):19–28.
[19] Kouremenos DA, Antonopoulos KA. Ambient temperature correlations in 35 locations in Greece (in Greek). Athens: Fivos Edn.; 1985.
[20] ASHRAE Handbook, Fundamentals volume, 1981.